International Journal of Structural Stability and Dynamics
(2022) 2250185 (21 pages)

DOI: 10.1142/S0219455422501851

Analysis of the Fluid–Structure Coupling Characteristics of a High-Speed Train Passing through a Tunnel

Zhanling Ji

Institute of Mechanics, Chinese Academy of Sciences
Key Laboratory for Mechanics in Fluid Solid Coupling Systems
No. 15 North 4th Ring West Road, Haidian District
Beijing 100190, P. R. China
149018663@qq.com

Wen Liu*

CRRC Industrial Academy Corporation Limited
Yard 1, Automobile Museum East Road
Fengtai District, Beijing 100070, P. R. China
liuwen@crrcgc.cc

Dilong Guo† and Guowei Yang‡

Institute of Mechanics, Chinese Academy of Sciences
Key Laboratory for Mechanics in Fluid Solid Coupling Systems
No. 15 North 4th Ring West Road, Haidian District
Beijing 100190, P. R. China
†*guodl@imech.ac.cn*
‡*gwyang@imech.ac.cn*

Jun Mao

School of Civil Engineering
Beijing Jiaotong University
No. 3 Shangyuan Village, Xizhimen
Haidian District, Beijing 100044, P. R. China
jmao@bjtu.edu.cn

Received 16 February 2022
Accepted 22 May 2022
Published 29 July 2022

After increasing the train speed, the wheel-rail coupling effect is intensified, as is the coupling effect between the train and the surrounding air, which causes the severe vibration of the train. Considering this problem and taking the high-speed train as the object of this study, a method for the coupling of aerodynamics and vehicle dynamics is proposed. Its validity is then demonstrated by the results of field tests and moving model experiments. On this basis, the

*Corresponding author.

fluid–structure coupling characteristics of a high-speed train passing through a tunnel are studied, as well as the effects of different coupling methods and track irregularities. The obtained results demonstrate that the interaction between the tail car and the surrounding air is significant. In the tunnel and at its exit, the lift and the car body acceleration significantly change, especially when the coupling of aerodynamics and vehicle dynamics, as well as the vertical and lateral track irregularities, are simultaneously imposed. When the head car travels out of the tunnel, the lift of the middle and tail cars both dramatically will change. It is deduced that the fluid–structure interaction has a significant effect on the swing phenomenon of the tail car. This phenomenon is the result of the combined effects of aerodynamics and track irregularities. The different frequencies of the lateral displacement for each car body, except the frequencies of the car bodies themselves, are mainly determined by vertical track irregularities.

Keywords: High-speed train; fluid–structure coupling; coupled aerodynamics and vehicle dynamics; passing through a tunnel; track irregularities.

1. Introduction

The operation of high-speed trains provides people with a convenient, fast, environmentally friendly, punctual, and safe way to travel. It has become a significant mode of transportation in many countries. With the increase of social progress and economic development, the number of people travelling between cities has increased by leaps and bounds. However, this is coupled with the uneven distribution of the population and resources in China. Improving the speed of trains is of great significance for the alleviation of the transportation pressure of people and goods, and for the promotion of economic and cultural exchanges. High-speed trains run on fixed lines at high speeds. They have a much higher slenderness ratio than other means of transportation, as well as a strong ground effect. These factors introduce several problems, the increasingly significant dynamic effect of the air around the train and intensified wheel-rail interactions, for example. In fact, China is a mountainous country with a relatively high railway tunnel line ratio. When trains pass through tunnels, the effects of the tunnel entrance and exit, aerodynamic drag, and sharp pressure changes occur, which affects the dynamic performance of the train during operation. Thus, the fluid–structure coupling effect has been widely studied.

Several studies have been performed on the aerodynamics and vehicle dynamics of high-speed trains, and remarkable achievements have been made. For instance, using the improved delayed separation vortex simulation method, Guo *et al.*[1] study the aerodynamic performance of high-speed trains with barriers with different ground clearance. Iyer *et al.*[2] explore the impacts of the blocking ratio and vehicle speed on the propagation characteristics of compressional waves. Li *et al.*[3] discuss the differences in the aerodynamic performance of a train passing through a long tunnel and two short tunnels with small gaps. Wang *et al.*[4] study the aerodynamic performance and flow-field evolution laws of high-speed trains under the effect of crosswind at a tunnel exit. However, in these studies, only an aerodynamic analysis is performed. Luo *et al.*[5] extend the traditional vehicle-track coupling theory through the coupling relationship between the track flexibility and the three-dimensional slab track

system. They also analyze and compare the dynamic response of the old and new models. Peixer *et al.*[6] evaluate the safety of high-speed trains running on viaducts under different track conditions. Jiang *et al.*[7] perform the stochastic dynamics analysis of a nonlinear vehicle-rail-bridge system using the Karhunen–Loève theorem and PEM method. Wu *et al.*[8] study the low-frequency swing of a car body based on a wheel-rail contact. Chen *et al.*[9] conduct the investigations on the effect of the polygonal wheel wear of high-speed trains. Gou *et al.*[10] study the influences of different types of bridge deformation on the dynamic response of high-speed trains. However, in these studies, the influence of aerodynamic loads is not considered.

Train derailment and overturning accidents caused by strong environmental wind and train wind are common. They seriously threaten the safe operation of trains. At present, aerodynamic loads are often applied as time-varying external loads, and the influence of the changes in the vehicle attitude on the surrounding flow field is not considered. For instance, Montenegro *et al.*[11] study the dynamic effect of a train-bridge system by generating random wind through a random wind velocity field. Wang *et al.*[12] analyze the dynamic response of the vehicle-track system by considering the comprehensive wind loads of train wind and crosswind, as well as track irregularities, as external excitations. Based on an unsteady simulation and decomposed slip grid technology, Chen *et al.*[13] analyze the aerodynamic and dynamic behaviors of a train near a slender hill next to a windbreak, under the effect of crosswind. Yao *et al.*[14] propose a new unsteady crosswind prediction formula which considers the complete turbulent field effect. They then use the virtual excitation method to calculate the power spectrum of the train response. Gou *et al.*[15] study the dynamic response of a vehicle-rail-bridge system running on a bridge at high speed, under different wind speeds and rainfall intensities. Wang *et al.*[16] analyze the influence of aerodynamic loads and wheel–rail contact on the nonlinear stability of HST. Sun *et al.*[17] simulate the aerodynamic forces of moving vehicles with dynamic mesh techniques. In addition, they study the characteristics of the wind environment on the bridge deck, in order to evaluate the driving safety and determine the influence coefficient. Huang *et al.*[18] apply the local proximity search method to unidirectional fluid-solid data exchange, under the condition of the mismatch between the fluid and structural grids after domain decomposition. For mismatched grids, Dou *et al.*[19] propose a method to transfer data from fluids to solids, based on the radial basis function and weight coefficient. However, the unidirectional aerodynamic and dynamic coupling ignores the change of the running attitude of the train under the force of the flow field, and cannot reflect the coupling relationship between the aerodynamics and vehicle dynamics. Thus, it is difficult to reveal the law of flow-induced vibration and reflect its essence.

The interactive co-simulation method considers the coupling effect between aerodynamics and the vehicle-track coupling dynamics of the high-speed train. It alternately calculates the high-speed train aerodynamics and the high-speed train system dynamics in the iterative calculation process.

Considering the coupling between the train and air, Nakade *et al.*[20] study the lateral vibration of a high-speed train passing through a tunnel. Based on an aerodynamic calculation software and a self-developed program of vehicle-track coupling dynamics, Li *et al.*[21,22] propose an embedded fluid–structure coupling co-simulation method and an equilibrium state method for high-speed trains, allowing to solve the interaction between the air and car bodies under the effect of the open-air crosswind. In this approach, the spring approximation method and grid remeshing method are used for the grid updating technology. More precisely, when the spring approximation method fails, the grid is updated by the remeshing method, and a grid reconstruction is performed. Zhai *et al.*[23] use the arbitrary Lagrangian-Euler method to deal with the dynamic boundary of the train and air. They also analyze the dynamic behavior of a high-speed train running on a track under the effect of crosswind, and control the train travelling in the crosswind by the head car. In this approach, the loose coupling method is used, and the head, middle and tail cars are integrated. When a train passes through a tunnel, in order to consider the interaction between the train and air, as well as to improve the calculation accuracy and stability of the whole system, it is necessary to develop an efficient and fully implicit method for coupling between the aerodynamics and vehicle dynamics.

In summary, considering the interaction between the train and the surrounding air, as well as the influences of the track irregularities and the tunnel effect, a fluid–structure vehicle-line-air coupling model is developed through the coupling of aerodynamics and vehicle dynamics. In addition, a grid motion approach which combines the overset grid method and user-defined grid motion, is proposed. Investigations of the fluid–structure interaction characteristics are performed under the condition of a train passing through a tunnel, including the aerodynamic characteristics, vertical vibration characteristics and lateral vibration characteristics.

2. Mathematical Model

The high-speed train coupling system is illustrated in Fig. 1. It includes wheel-rail interaction exacerbated by track irregularities, fluid–structure interaction caused by traveling wind and ambient wind, and pantograph-catenary interaction. After the train speed increases, the aerodynamic effect is more prominent, different excitation responses are more sensitive, and the interactions among the high-speed train, line, air and catenary are enhanced. Consequently, it is necessary to use new means and

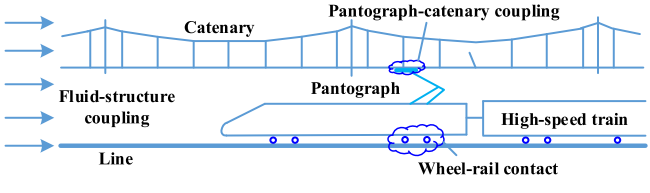

Fig. 1. Schematic diagram of the coupling system of a high-speed train.

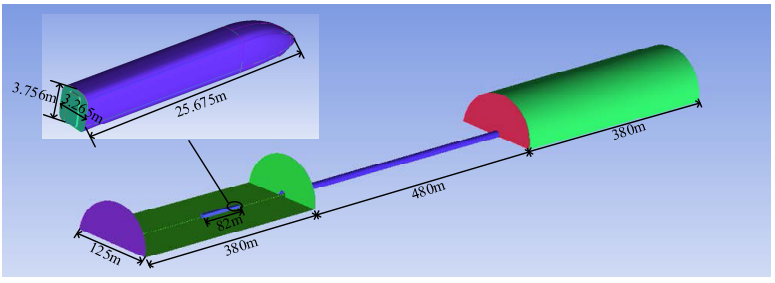

Fig. 2. Geometric model of a fluid field passing through a tunnel.

methods in order to perform further studies. Due to the large mass of the vehicle, the pantograph-catenary system has little influence on the vehicle. Thus, only the interactions among the vehicle, line and air are considered.

The geometric model of fluid field passing through a tunnel is shown in Fig. 2. Its main dynamic parameters are presented in Table 1. The power spectral density (PSD) curve of the vertical track irregularities is shown in Fig. 3.

2.1. *Vehicle dynamics model*

The high-speed train comprises three groups: the head car, middle car and tail car. Each car is mainly composed of a car body and two bogies, while each bogie includes

Table 1. Main dynamic parameters of the train.

Parameter	Value	Unit
Distance between bogie centers of one unit	17.375	m
Wheelbase	2.5	m
Lateral span of wheel rolling circle	1.493	m
Diameter of wheel rolling circle	0.92	m
Distance between the backs of the wheel flanges	1.353	m
Wheel profile	S1002G	—
Rail mass per unit length	60	kg/m
Mass of car body	38 884	kg
Roll inertia of car body	1 259 000	$N \cdot m^2$
Pitch inertia of car body	19 053 000	$N \cdot m^2$
Yaw inertia of car body	17 979 000	$N \cdot m^2$
Gravity center height of car body	1.656	m
Longitudinal stiffness of a primary spring	919 800	N/m
Lateral stiffness of a primary spring	919 800	N/m
Vertical stiffness of a primary spring	886 005	N/m
Damping of a primary vertical damper	10 000	$N \cdot s/m$
Joint stiffness of a primary vertical damper	7 500 000	N/m
Longitudinal stiffness of an axle box rotary arm joint	120 000 000	N/m
Lateral stiffness of an axle box rotary arm joint	12 500 000	N/m
Damping of an anti-yaw damper	225 000	$N \cdot s/m$
Joint stiffness of an anti-yaw damper	35 000 000	N/m

Table 1. (*Continued*)

Parameter	Value	Unit
Longitudinal stiffness of a secondary air spring	133 000	N/m
Lateral stiffness of a secondary air spring	133 000	N/m
Vertical stiffness of a secondary air spring	203 000	N/m
Damping of a secondary vertical damper	10 000	N · s/m
Joint stiffness of a secondary vertical damper	5 000 000	N/m
Damping of a secondary lateral damper	15 000	N · s/m
Joint stiffness of a secondary lateral damper	4 250 000	N/m
Free clearance of a lateral stop	0.02	m
Roll angle stiffness of the anti-roll rod	4 150 000	N · m/rad

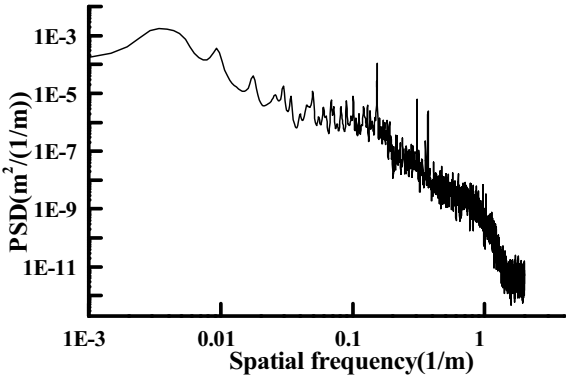

Fig. 3. PSD curve of the vertical track irregularities.

a frame, four axle boxes, front and rear wheelsets. The different parts of the vehicle are connected and transmitted through the primary and secondary suspension systems, and the cars are connected by hooks. In the vehicle dynamics model, the car body, bogie, wheelset and axle box are all considered as rigid bodies. The car body, bogie and wheelset are considered to have five degrees of freedom (DOFs) of lateral movement, vertical movement, rolling, shaking and nodding. The axle box is considered to have one DOF of nodding. In addition, the nonlinear characteristics of the primary and secondary suspension systems are considered.

The vibration differential equation of the vehicle system is given by

$$[M]\{\ddot{u}\} + [C]\{\dot{u}\} + [K]\{u\} = \{Q\}, \tag{2.1}$$

where $[M]$ is the mass matrix, $[C]$ is the damping matrix, $[K]$ is the stiffness matrix, $\{u\}$ is the displacement vector, and $\{Q\}$ is the dynamic load vector caused by the gravity and track irregularities, while for the car body, also including aerodynamic loads.

2.2. *Fluid governing equation*

Regardless of the mass force, in the rectangular coordinate system, the conservation Navier–Stokes (N-S) equation can be written in vector form:

$$\frac{\partial U}{\partial t}+\frac{\partial(E-E_v)}{\partial x}+\frac{\partial(F-F_v)}{\partial y}+\frac{\partial(G-G_v)}{\partial z}=0, \tag{2.2}$$

where:

$$U=\begin{pmatrix}\rho\\ \rho u\\ \rho v\\ \rho w\\ \rho e\end{pmatrix},\quad E=\begin{pmatrix}\rho u\\ \rho u^2+p\\ \rho uv\\ \rho uw\\ (\rho e+p)u\end{pmatrix},\quad F=\begin{pmatrix}\rho v\\ \rho vu\\ \rho v^2+p\\ \rho vw\\ (\rho e+p)v\end{pmatrix},\quad G=\begin{pmatrix}\rho w\\ \rho uw\\ \rho vw\\ \rho w^2+p\\ (\rho e+p)w\end{pmatrix},$$

$$E_v=\begin{pmatrix}0\\ \tau_{xx}\\ \tau_{xy}\\ \tau_{xz}\\ u\tau_{xx}+v\tau_{xy}+w\tau_{xz}+k\dfrac{\partial T}{\partial x}\end{pmatrix},\quad F_v=\begin{pmatrix}0\\ \tau_{xy}\\ \tau_{yy}\\ \tau_{yz}\\ u\tau_{xy}+v\tau_{yy}+w\tau_{yz}+k\dfrac{\partial T}{\partial y}\end{pmatrix},$$

and

$$G_v=\begin{pmatrix}0\\ \tau_{xz}\\ \tau_{zy}\\ \tau_{zz}\\ u\tau_{xz}+v\tau_{zy}+w\tau_{zz}+k\dfrac{\partial T}{\partial z}\end{pmatrix},$$

where t is the time, ρ is the density, p is the pressure, u is the velocity in the x-direction, v is the velocity in the y-direction, w is the velocity in the z-direction, μ is the viscosity, T is the temperature, k is the heat conduction coefficient, e is the total energy per gas mass, τ_{xx}, τ_{xy}, τ_{yx}, τ_{yy}, τ_{zz}, τ_{yz}, τ_{zy}, τ_{xz} and τ_{zx} are the shear stresses in different planes.

3. Coupling Method of Aerodynamics and Vehicle Dynamics

3.1. *Coupling principle*

The dual-time-step method is used for the coupling of the aerodynamics and vehicle dynamics. That is, each physical time step is divided into multiple sub-iterations. In each sub-iteration, the unsteady aerodynamic loads are first calculated using the computational fluid dynamics (CFD) method. The aerodynamic loads are then transferred to the structural model using the data exchange method. The structural motion under unsteady aerodynamic loads is obtained by solving the dynamics

equation. The structural displacement is then transferred to the aerodynamic model. According to the transferred structural displacement, the aerodynamic grid is updated by combining the overset method and user-defined grid motion. When the calculation accuracy reaches the predetermined accuracy or the number of iterations reaches the predetermined number, the sub-iteration calculation is completed. Afterwards, the next sub-iteration of the unsteady aerodynamic load calculation process is initiated. The flow-field information and node positions of the next physical time step are then updated. This process is repeated until the problem analysis is completed. At this time, the data exchanged at a given time point can be approximately considered as the data of the current time step. Therefore, the interactive mode is mainly real-time. The flow is shown in Fig. 4.

3.2. *Key coupling technologies*

Due to the large size and rigidity of the car body, the impacts of the aerodynamic loads on its attitude change are varied, while there is little influence on its deformation. Therefore, the car body is considered as a rigid body, and the interaction between the aerodynamic force and the attitude change of the car body is considered. In the coupling of the fluid and the rigid body structure, the solid deformation is ignored, and only the grid motion of the flow field caused by attitude changes is considered. For a single car body, considering the six DOFs of motion, the overset method has unique advantages, compared with other grid motion methods. In the overset method, there is no grid reconstruction, and the grid quality is not affected. The multi-region grid division is used, and the complex geometry is decomposed into simple systems with overset grids, which makes the control of the grid quality easier. In summary, the overset method has substantial advantages in the simulation of the fluid–structure coupling of large models with multiple DOFs. Moreover, the

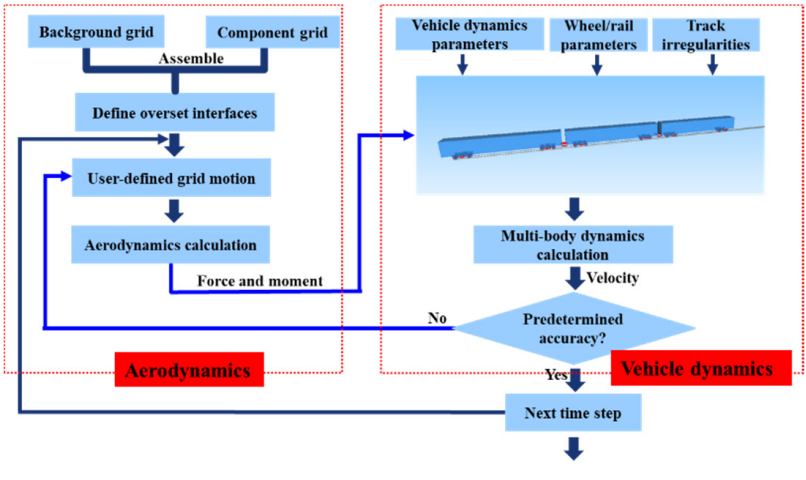

Fig. 4. Flowchart of the coupling of aerodynamics and vehicle dynamics.

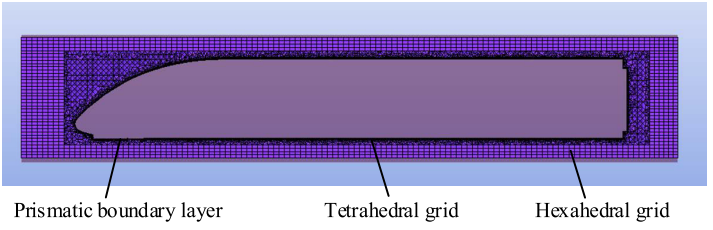

Fig. 5. Hybrid meshing.

user-defined grid motion is suitable for the component fluid field around the train caused by changes in the train attitude. Therefore, the grid motion technology which combines the overset method and user-defined grid motion, is used for the car body.

According to the requirements of the coupling method of aerodynamics and vehicle dynamics, a hybrid meshing method is used for the flow field around the train, as shown in Fig. 5. Prismatic boundary layers are used near the train surface, which describes the motion of the boundary layer and considers the surface viscous force. The train shape is complex, and a tetrahedral grid is used outside the boundary layer, which is convenient for meshing. A hexahedral grid is used for the outermost part, as it is regular and easy to control, and it matches the tunnel flow-field grid. A hexahedral grid is also used for the flow field inside and outside the tunnel, as it is regular and easy to control. By matching the hexahedral grid around the train with that inside and outside the tunnel, the isolated elements can be avoided. Finally, the flow fields around the three cars are used as the component grids, the flow field inside and outside the tunnel is used as the background grid, and the four grids are assembled, as shown in Fig. 6. The developed aerodynamic calculation model is shown in Fig. 7.

In CFD, after reading the six-degrees-of-freedom (6DOF) velocities of each car body calculated by vehicle dynamics, they are assigned to the three component fluid fields. Therefore, the motions of the three components are performed, and the unsteady aerodynamic characteristics are induced.

A three-group train is used. It includes a head, middle and tail cars, that are rigid bodies. Considering the influences of track irregularities and aerodynamic forces, the existing dynamic vehicle and track parameters are applied, and the multi-level substructure modeling method is used, as shown in Fig. 8. The developed dynamic vehicle model is shown in Fig. 9. The car body is assembled with the bogie by a

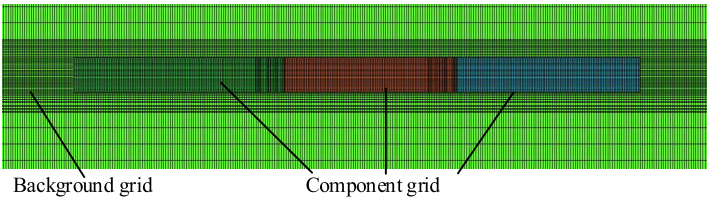

Fig. 6. Overset grid.

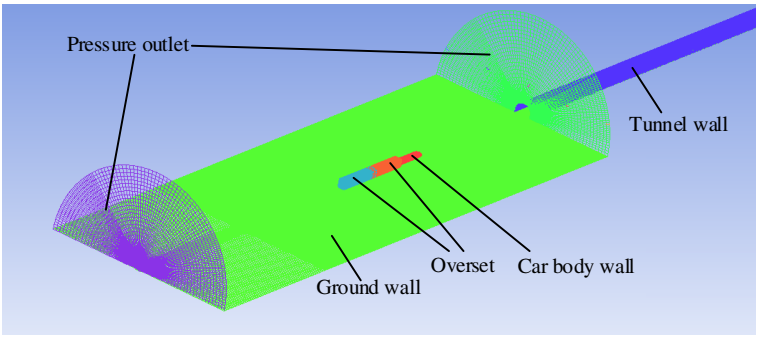

Fig. 7. Model for aerodynamic calculations.

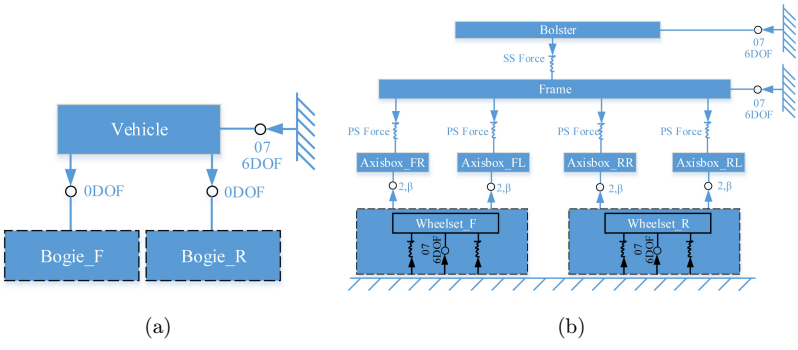

(a) (b)

Fig. 8. The model topology of a high-speed train. (a) The main model topology. (b) The bogie substructure topology.

bolster, and it is articulated with the system by a six-DOF joint. The bolster is fixed with the car body and connected with the bogie by spring-damping force elements in order to simulate air springs. The wheelset and the system are connected by a No. 7 general rail track joint with six DOFs. The connection between the wheel and rail is generated after the geometric contact relationship between them is set. The primary and secondary suspension devices and shock absorbers in the model are simplified as

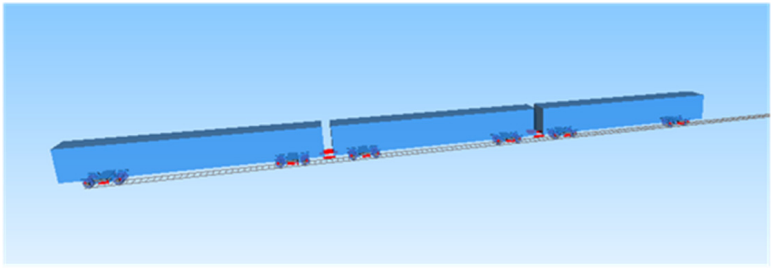

Fig. 9. The coupled vehicle-line dynamics model.

force elements during modeling. In order to develop the vehicle dynamics model for fluid–structure coupling, all the aerodynamic loads are set as substitution variables, and they are continuously updated by overwriting them.

In the proposed method for the coupling of the aerodynamics and vehicle dynamics, different meshing methods are used for different regions of the flow field. This allows the full consideration of the surface viscous force, and better simulates the boundary layer effect. Moreover, it is easier to divide and control the meshing, and the grid quality remains unchanged during motion. The grid motion technology, which combines the overset grid method and user-defined grid motion, is used to better complete the combination of the overall large-scale longitudinal motion and local small-scale attitude changes of the car body. Data transfer between two physical fields is performed through data files, which is simple, quick and easy to implement, and it can ensure data reliability.

The Fluent software is used in fluid simulation, and the Simpack software is used in vehicle dynamics simulation. The co-simulation between aerodynamics and vehicle dynamics is implemented using Fluent udf self-developed, in which data exchange is performed by reading result files. According to the results, all the node locations of the three component fluid fields are updated, and the vehicle is imposed by the aerodynamic forces, that are updated using the results read to overwrite the substitution variables.

3.3. *Verification of the coupling method*

Figure 10 presents the vertical acceleration of the car body and its PSD curves during a simulation and a test. In the dynamic simulation, the research object is three cars, the track irregularities of the Beijing–Tianjin line are applied, the calculation case is open-air running, and the coupling of aerodynamics and vehicle dynamics is considered. The test results are the field test results of trains from Beijing

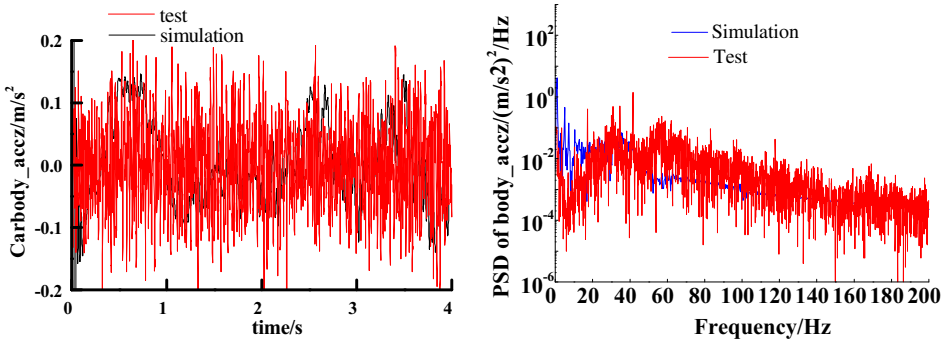

(a) (b)

Fig. 10. Vertical acceleration and its PSD of the car body during the simulation and test. (a) Vertical carbody acceleration. (b) Vertical acceleration PSD of the car body.

to Tianjin. When the test is performed, the train is in a stable state, i.e. the processes of starting acceleration and braking deceleration are not included. For comparison with the test results, the starting acceleration stage is removed when the simulation results are drawn. It can be seen from Fig. 10 that the simulation results are mainly consistent with the test results. However, there are some certain differences, especially below 20 Hz. These differences occur mainly because the simulation conditions are not exactly same as the test conditions, such as the random wind, the elastic deformations of the track and subgrade, and other disturbances in the natural environment.

For open air and tunnel cases, some are completely the same, such as the vehicle dynamics model, the aerodynamic component grids of the head, middle and tail cars, the meshing method and sizes of the aerodynamic background grids, and the coupling method. Only the background grid shape in the flow field is different. The verification of the calculation results of open-air case shows that the completely same parts are right and valid.

The pressure curves of the nose cone of the head car from a moving model experiment rig and the coupling simulation calculation were shown as Figs. 11(a) and 11(b), respectively. The two are under the case of passing through a tunnel and at the same speed, and the cross-section area of the tunnels are same. But the scaling factors of the tunnel length and the train model on the experiment rig is 1:8. From the comparison between Figs. 11(a) and 11(b), they are basically consistent. Their differences mainly resulted from the incompletely same between the model on the experiment rig and the model used in simulation calculation. The train on the experiment rig is mainly used to test aerodynamic pressure.

Figure 12 shows the pressure curve of monitoring point hb on the head car body (cf. Fig. 15), passing through a tunnel and pressure wave propagation in the tunnel during the coupling simulation calculation. At ①, after the tail car enters the tunnel, the initial expansion wave propagates forward to the monitoring point at the sound

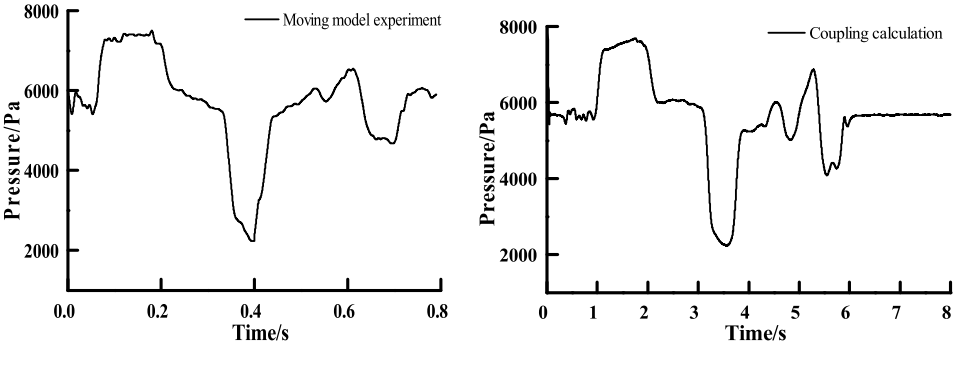

Fig. 11. The pressure curves of the nose cone of the head car. (a) From the moving model experiment rig. (b) From the coupling simulation calculation.

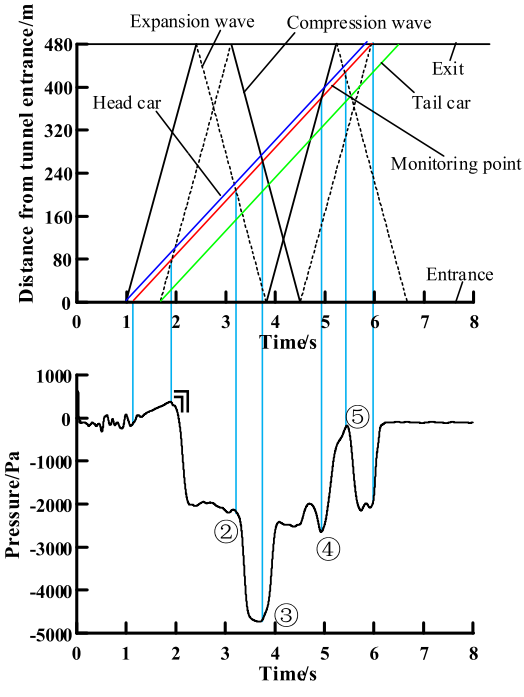

Fig. 12. Pressure curve of monitoring point hb on the head car body and pressure wave propagation in the tunnel.

speed, which makes the pressure at the point sharply decrease. At ②, after the head enters the tunnel, the initial compression wave propagates to the tunnel exit, the reflected expansion wave returns and propagates to the monitoring point, which makes the pressure at the point sharply decrease again. At ③, the initial expansion wave propagates to the tunnel exit, the compression wave generated by reflection returns and propagates to the monitoring point, which causes the pressure at the point to sharply increase. At ④, the initial compression wave propagates to the tunnel exit, the expansion wave generated by reflection returns to the tunnel entrance, and the generated compression wave propagates to the monitoring point, which causes the pressure at the point to rapidly increase. At ⑤, the initial compression wave propagates to the tunnel exit, the second reflected expansion wave reaches the monitoring point, which causes the pressure at the point to sharply decrease. It can be seen there is tight corresponding relationship between the pressure change at the monitoring point and the pressure wave propagation in the tunnel, which also demonstrates that the tunnel aerodynamic model is right.

3.4. *Verification of grid independence*

In order to verify the grid independence for aerodynamic calculation, the fluid field of a high-speed train passing through a tunnel is divided into three sets of grids.

Table 2. Aerodynamic coefficients of the car bodies with different grid numbers in the flow field.

	C_d-head car body	C_d-middle car body	C_d-tail car body	Total C_d
Fine mesh	−0.085	−0.062	−0.072	−0.219
Medium mesh	−0.086	−0.064	−0.074	−0.224
Coarse mesh	−0.081	−0.069	−0.076	−0.226

The total cells are almost 23.5 million, 20 million and 15.7 million, respectively. At the stable stage of open air, the calculation results for drag coefficient from each car body are shown in Table 2. The results of the medium grid are closer to that of the fine grid than the coarse grid. Therefore, in order to ensure the computational accuracy and improve the calculation efficiency, a medium grid is used for all the subsequent analyses, in which the grid size of the car body surface is 0.128 m, its boundary layer number is 10, the initial boundary layer height is 0.8 mm and the height ratio is 1.5. The longitudinal grid size of the component surface is 0.256 m, and its cross-section grid size is 0.15 m. In the background region, in the tunnel and the area corresponding to the tunnel, the longitudinal grid size is 0.325 m, and the cross-section grid size is 0.15 m.

4. Results and Discussion

The calculation case is a train passing through a tunnel, which is a Chinese standard single-track tunnel having a cross-sectional area of 70 m^2. The train speed is 360 km/h, and the unfavorable tunnel length is 480 m. Due to the fact that the primary focus is on the coupling between the aerodynamics and the multi-body dynamics of the car body, in the fluid calculation, the high-speed train is simplified by ignoring the air conditioning, the pantograph and the bogie. The flow field is three-dimensional, viscous, compressible, with unsteady turbulent flow. The flow medium is set as air (ideal gas), and the turbulence model is the shear stress transport (SST) $k-\omega$ model. The boundary conditions of the flow field are as follows: the car body surface is set as the non-slip boundary with friction, the ground and tunnel wall are fixed walls, the outside boundary of the calculation area is set as the pressure outlet, the outlet pressure is set to standard atmospheric pressure, and the boundaries of the three components are set to overset (cf. Fig. 7). Because the three car bodies have their own 6-DOF displacements, in order to achieve the coupling of the aerodynamics and vehicle dynamics, in the aerodynamic calculation, cuts are made at the windshields between cars.

4.1. *Influence of different coupling methods*

Figure 13 presents the car-body coupling characteristics while passing through a tunnel and considering both vertical and lateral track irregularities. It also shows the influence of different coupling methods, such as no wind load, aerodynamic loads as the known loads, and the coupling of the aerodynamics and vehicle dynamics. In no

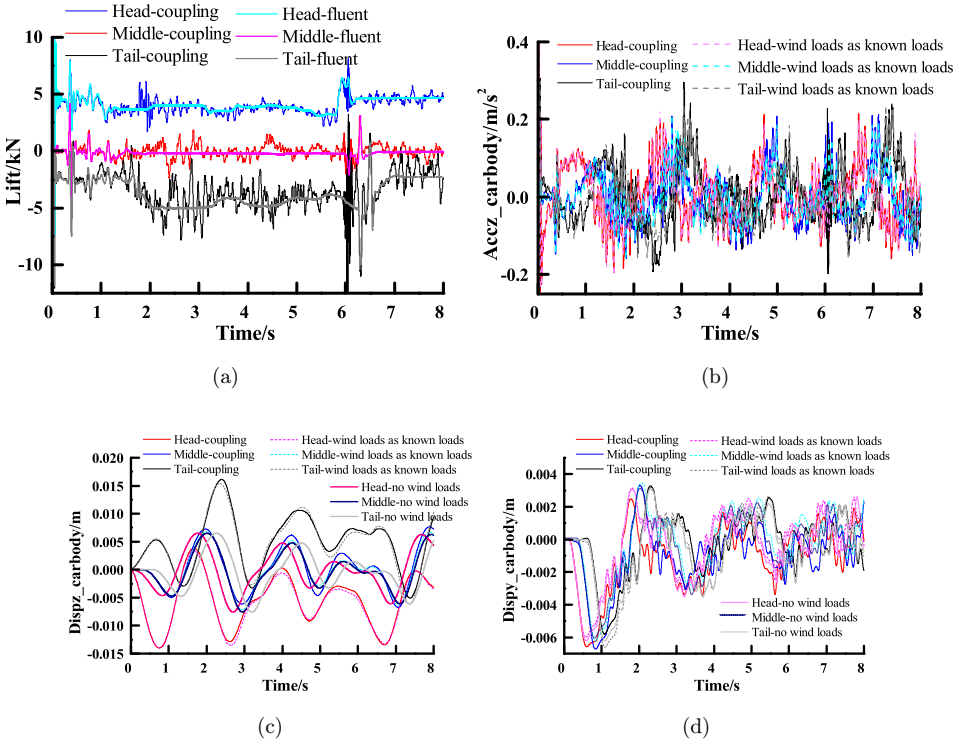

Fig. 13. Coupling characteristics of the three car bodies using different coupling methods. (a) Lift. (b) Vertical acceleration. (c) Vertical displacement. (d) Lateral displacement.

wind load, only vertical and lateral track irregularities are considered, while aerodynamic loads are not considered. In aerodynamic loads as the known loads, aerodynamic loads are first calculated in CFD, and then applied to vehicle dynamics as the known loads. In the coupling of the aerodynamics and vehicle dynamics, for each sub-iteration, aerodynamic loads and velocities are exchanged. By comparing and analyzing these curves, the main conclusions are drawn as follows.

- Compared with the purely aerodynamic calculation, the change law and direction of the lift of each car are mainly the same during coupling. That is, the head car is under downward pressure, the middle car is under downward pressure or upward floating force, and the tail car is basically under upward floating force. However, the lift fluctuation ranges are much larger, and sequentially increased from the head car to the middle car, and finally to the tail car. For example, in the purely aerodynamic calculation, the sudden change amplitudes of the lift at the tunnel exit are, respectively, 3.4 kN, 4.4 kN and 10.7 kN, while in the coupling calculation, these values are, respectively, 5.8 kN, 4.5 kN and 12.6 kN. When the head car drives out of the tunnel, the lifts of the middle and tail cars suddenly change during

coupling, and the amplitudes are, respectively, 5.25 kN and 18.6 kN (the amplitude for the tail car is particularly high).

- The vertical accelerations generally increase sequentially from the head car to the middle car, and finally to the tail car. When the head car is at the tunnel exit, all the vertical accelerations of the three cars are higher. When the middle and tail cars are, respectively, at the tunnel exit, their vertical accelerations are also higher. The maximum vertical acceleration of the tail car, which is $0.296\,\mathrm{m/s^2}$, occurs at 3.05 s. However, this is not the time of the maximum value of its lift. Thus, it is evident that while lift is a crucial factor that affects the vertical acceleration, it is not the only influencing factor.
- Compared with the case without considering wind loads, when the aerodynamic loads are taken as known loads and the aerodynamics and vehicle dynamics are coupled, the vertical displacement of the head and tail cars substantially increase, while that of the middle car changes little. For example, near 2.35 s, the vertical displacement of the tail car increases from 0.0065 m to 0.0154 m and 0.016 m, respectively. Near 2.65 s, the vertical displacement of the head car increases from 0.0077 m to 0.0136 m and 0.0128 m, respectively. Near 3.0 s, the vertical displacement of the middle car increases from 0.0066 m to 0.0068 m and 0.0073 m, respectively. Compared with the case of considering the aerodynamic loads as known loads, the vertical displacement of each car sometimes increases and sometimes decreases during coupling. It can be seen the coupling causes the calculation results to be closer to objective reality, and does not necessarily increase the results. For example, at 4.5 s, the vertical displacement of the tail car decreases from 0.0112 m to 0.0105 m, while at 2.65 s, the vertical displacement of the head car decreases from 0.0136 m to 0.0128 m.
- Compared with the case without considering wind loads, when the aerodynamic loads are taken as known loads and the aerodynamics and vehicle dynamics are coupled, the changes of the lateral displacement of the head and tail cars are much smaller than those of the vertical displacement. For example, near 2.35 s, the vertical displacement of the tail car changes from 0.0065 m to 0.0154 m and 0.016 m, respectively. In addition, near 2.31 s, the lateral displacement of the tail car changes from 0.0031 m to 0.0032 m and 0.0033 m, respectively. Near 2.65 s, the vertical displacement of the head car changes from 0.0077 m to 0.0136 m and 0.0128 m, respectively. Moreover, near 1.8 s, the lateral displacement of the head car changes from 0.0031 m to 0.0032 m and 0.0025 m, respectively.

4.2. *Influences of vertical and lateral track irregularities under fluid–structure coupling*

Figure 14 presents the coupling characteristics of three car bodies with only vertical track irregularities and with both vertical and lateral track irregularities, while passing through a tunnel, and when considering the coupling of the aerodynamics

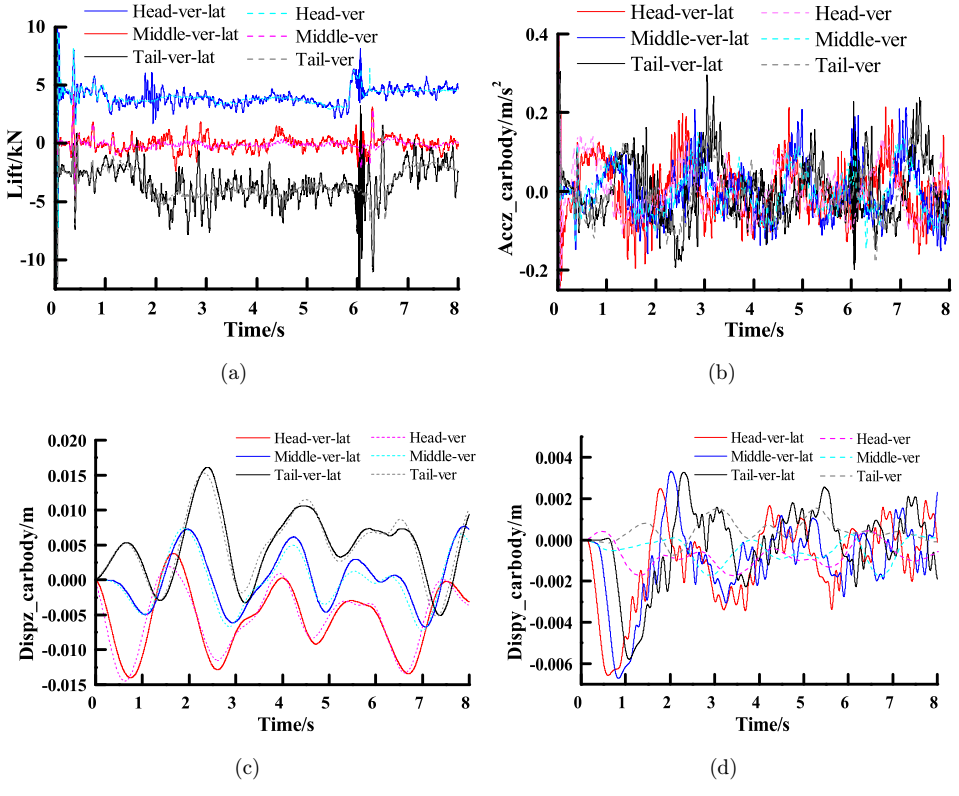

Fig. 14. Coupling characteristics of three car bodies under different track irregularities. (a) Lift. (b) Vertical acceleration. (c) Vertical displacement. (d) Lateral displacement.

and vehicle dynamics. By comparing and analyzing these curves, the main conclusions are drawn as follows:

- Compared with the case in which only vertical track irregularities are applied, in the case where vertical and lateral track irregularities are simultaneously applied, the change laws and direction of the lift of each car are mainly the same. However, the fluctuation amplitudes are much higher and sequentially increase from the head car to the middle car, and finally to the tail car. For example, at the tunnel exit, when only vertical track irregularities are applied, the abrupt lift amplitudes are, respectively, 3.3 kN, 5 kN and 11.3 kN. When vertical and lateral track irregularities are simultaneously applied, the abrupt lift amplitudes are, respectively, 5.8 kN, 4.5 kN and 12.6 kN. Compared with the case in which only vertical track irregularities are applied, in the case where vertical and lateral track irregularities are simultaneously applied, the abrupt change amplitudes of the lift of the middle and tail cars when the head car is leaving the tunnel are higher than those when the middle and tail cars are exiting the tunnel. Compared with the case of considering the aerodynamic loads as the known loads presented in Fig. 12(a),

the frequency and amplitude of the lift of each car are higher when only vertical track irregularities are applied.

- Compared with the case where only vertical track irregularities are applied, in the case where vertical and lateral track irregularities are simultaneously applied, the vertical acceleration of each car mostly increases. For example, the maximum acceleration of the head car increases from $0.149\,\mathrm{m/s^2}$ to $0.213\,\mathrm{m/s^2}$, which denotes an increase of 42.95%, that of the middle car increases from $0.147\,\mathrm{m/s^2}$ to $0.211\,\mathrm{m/s^2}$, which represents an increase of 43.53%, and finally, that of the tail car increases from $0.195\,\mathrm{m/s^2}$ to $0.296\,\mathrm{m/s^2}$, which denotes an increase of 51.79%.
- Compared with the case where only vertical track irregularities are applied, in the case where vertical and lateral track irregularities are simultaneously applied, the vertical displacements of each car sometimes increase and sometimes decrease. For example, near 2.65 s, the vertical displacement of the head car increases from 0.0115 m to 0.0128 m. At 4.25 s, that of the middle car decreases from 0.0051 m to 0.0061 m. Finally, at 6.53 s, that of the tail car decreases from 0.0087 m to 0.0074 m.
- Compared with the case in which only vertical track irregularities are applied, in the case where vertical and lateral track irregularities are simultaneously applied, the main frequencies of the lateral displacement of each car body are mainly the same, but their amplitudes greatly increase. For example, at 1.78 s, the lateral displacement of the head car increases from 0.0008 m to 0.0025 m, at 2.03 s, that of the middle car increases from 0.0001 m to 0.0033 m, and finally, at 2.3 s, that of the tail car increases from 0.0004 m to 0.0033 m. By comparing the case without wind load while simultaneously considering vertical and lateral track irregularities (cf. Fig. 12(d)) with the coupling cases shown in Fig. 13(d), it is deduced that the frequencies of the lateral displacement of each car body are mainly determined by vertical track irregularities, excluding the frequencies of the car body itself.
- The lateral track irregularities are inseparably coupled with vertical track irregularities, and they cannot be ignored.

4.3. *Swing phenomenon of the tail car*

When the train travel at high speeds, the serious swing phenomenon of the tail car often occurs. In order to clarify this phenomenon, Figs. 13 and 14 are comprehensively compared and analyzed. The lift of the tail car is basically upward. When coupling the aerodynamics and vehicle dynamics, and simultaneously applying vertical and lateral track irregularities, the fluctuation amplitudes of the lift of the tail car body are the highest among all the cars, especially before the head car enters the tunnel, when it is in the tunnel, and when it is at the tunnel exit, and when the tail car is at the tunnel exit. In addition, when coupling the aerodynamics and vehicle dynamics, and simultaneously applying vertical and lateral track irregularities, when the head car is near the tunnel exit (i.e. at 5.5–6.2 s), the lateral displacement directions of the head and middle cars are opposite to those of the tail car, and the

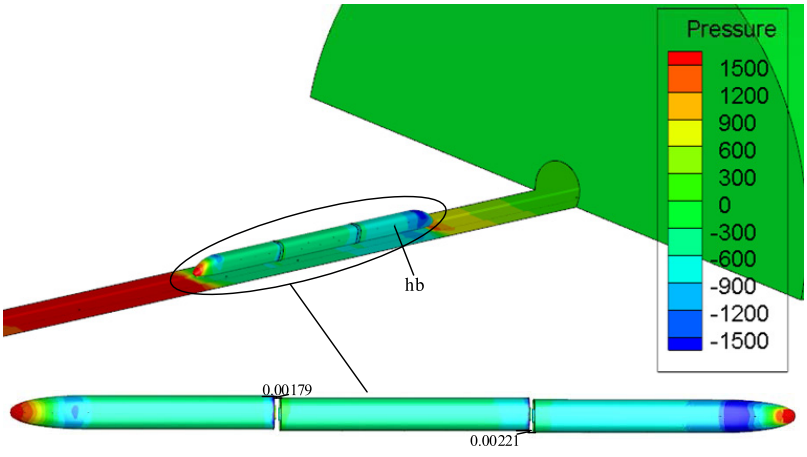

Fig. 15. Local pressure cloud diagram when the train is travelling for 5.4 s.

differences in the lateral displacement values are large. Consequently, when the head car drives out of the tunnel exit, the lift of the tail car suddenly changes and its amplitude is high. Finally, compared with the case where the wind loads are not considered, in the case of considering the aerodynamic loads as known loads and the case where the aerodynamics and vehicle dynamics are coupled, both the vertical upward displacement and lateral displacement significantly increase, which results in the swing phenomenon of the tail car. Thus, it is evident that the swing phenomenon of the tail car is the result of the combined effects of aerodynamics and track irregularities. Due to the windshield cuts, the magnitudes of the sudden change at this time may be larger than the actual magnitudes.

Figure 15 shows the local pressure cloud diagram when the train is travelling for 5.4 s. The pressure is higher for the tail car, while it is lower for the head car. This is opposite to that under open-air case. At the time, the lateral displacements of the head, middle and tail cars are 0.00221 m, −0.00068 m and −0.00179 m, respectively. They are opposite for the head car and the tail car and smaller for the middle car. Therefore, they induce the different vibrations of the car bodies.

5. Conclusions

In this paper, using a proposed aerodynamics and vehicle dynamics coupling method, a study is performed on the response characteristics of high-speed trains in tunnels to aerodynamic loads under different conditions. The main conclusions are summarized as follows:

- Considering the coupling of the aerodynamics and vehicle dynamics, as well as the simultaneous application of vertical and lateral track irregularities, when the head car drives out of the tunnel, sudden lift changes of the middle and tail cars occur, and their amplitudes are, respectively, 5.25 kN and 18.6 kN.

- The lateral displacement changes of the head and tail cars are much smaller than their vertical displacement changes, but the influence of lateral track irregularities is significant.
- The frequencies of the lateral displacement of each car are mainly determined by vertical track irregularities, excluding the frequencies of the car body itself.
- By investigating the coupling characteristics under different cases, the swing phenomenon of the tail car is deeply elaborated.

In future work, the aeroelastic research method will be used to seal the windshields between cars in the aerodynamic calculation, and the vehicle driving safety will be carried out using the developed method.

Acknowledgments

The authors gratefully acknowledge the support of the National Numerical Engieering Project (grant no. NNW2020-DY01-002), the National Science Foundation of China (grant no. 52172336), the Strategic Priority Research Program of the Chinese Academy of Sciences (Class B) (grant no. XDB22020000), the Research Project of Chinese Academy of Sciences (grant no. XXH13506-204), and the National Key Research & Development Projects (grant no. 2017YFB0202801).

References

1. Z. J. Guo *et al.*, Aerodynamic influence of the clearance under the cowcatcher of a high-speed train, *J. Wind Eng. Ind. Aerod.* **220** (2022) 104844.
2. R. S. Iyer, D. H. Kim and H. D. Kim, Propagation characteristics of compression wave in a high-speed railway tunnel, *Phys. Fluids* **33**(8) (2021) 086104.
3. W. Li *et al.*, Aerodynamic effects of a high-speed train travelling through adjoining & separated tunnels, *Tunn. Undergr. Sp. Tech.* **113** (2021) 103973.
4. L. Wang *et al.*, Aerodynamic performance and flow evolution of a high-speed train exiting a tunnel with crosswinds, *J. Wind Eng. Ind. Aerod.* **218** (2021) 1–14.
5. J. Luo, S. Y. Zhu and W. M. Zhai, An advanced train-slab track spatially coupled dynamics model: Theoretical methodologies and numerical applications, *J. Sound Vib.* **501** (2021) 1–30.
6. M. A. Peixer *et al.*, Running safety evaluation of a train moving over a high-speed railway viaduct under different track conditions, *Eng. Fail. Anal.* **121** (2021) 1–17.
7. L. Z. Jiang *et al.*, Application of KLE-PEM for random dynamic analysis of nonlinear train-track-bridge system, *Shock Vib.* **2020** (2020) 1–10.
8. Y. Wu *et al.*, Low-frequency carbody sway modelling based on low wheel-rail contact conicity analysis, *Shock Vib.* **2020** (2020) 1–17.
9. S. X. Chen and Y. T. Ni, Effect of wheel polygonalization on the degree of non-linearity of dynamic response of high-speed vehicle system, *Meas. Control* **54**(9–10) (2021) 1286–1300.
10. H. Y. Gou *et al.*, Dynamic responses of a high-speed train passing a deformed bridge using a vehicle-track-bridge coupled model, *Proc. Inst. Mech. Eng. F J. Rail Rapid Transit* **235**(4) (2021) 463–477.

11. P. A. Montenegro *et al.*, Dynamic effects on a train-bridge system caused by stochastically generated turbulent wind fields, *Eng. Struct.*, **211** (2020) 110430.
12. Y. Wang *et al.*, Coupling vibration response analysis of wind-train-bridge system considering the train-induced wind effect, *Wind Struct.* **33**(3) (2021) 217–231.
13. Z. Chen *et al.*, Aerodynamic performance and dynamic behaviors of a train passing through an elongated hillock region beside a windbreak under crosswinds and corresponding flow mitigation measures, *J. Wind Eng. Ind. Aerod.* **208** (2021) 104434.
14. Z. Yao and N. Zhang, Overturning assessment of railway vehicles under cross winds, *Wind Struct.* **33**(1) (2021) 1–11.
15. H. Y. Gou *et al.*, Dynamic response of high-speed train-track-bridge coupling system subjected to simultaneous wind and rain, *Int. J. Struct. Stab. Dyn.* **21**(11) (2021) 2150161.
16. J. C. Wang *et al.*, The influence of aerodynamic loads on carbody low-frequency hunting of high-speed trains, *Int. J. Struct. Stab. Dyn.* https://doi.org/10.1142/S0219455422501450.
17. M. J. Sun *et al.*, Simplified method for estimating the critical wind speed of moving vehicles on bridges under crosswinds, *Int. J. Struct. Stab. Dyn.* **22**(5) (2022) 2250046.
18. S. Huang *et al.*, A data exchange algorithm for one way fluid-structure interaction analysis and its application on high-speed train coupling interface, *J. Appl. Fluid Mech.* **11**(2) (2018) 519–526.
19. W. Dou *et al.*, A combined radial basis function based on interpolation method for fluid-structure interaction problems and its application on high-speed trains, *Adv. Eng. Softw.* **131** (2019) 143–152.
20. K. Nakade, S. Masahiro and F. Hiroshi, Interaction between vehicle vibration and aerodynamic force on high-speed train running in tunnel, *Vehicle Syst. Dyn.* **41** (2004) 717–723.
21. T. Li, J. Y. Zhang and W. H. Zhang, An improved algorithm for fluid-structure interaction of high-speed trains under crosswind, *J. Mod. Transport.* **19**(2) (2011) 75–81.
22. T. Li *et al.*, A fast equilibrium state approach to determine interaction between stochastic crosswinds and high-speed trains, *J. Wind Eng. Ind. Aerod.* **143** (2015) 91–104.
23. W. M. Zhai *et al.*, Dynamics of high-speed train in crosswinds based on an air-train-track interaction model, *Wind Struct.* **20**(2) (2015) 143–168.